# Palladium electrodissolution from model surfaces and nanoparticles

Enrico Pizzutilo[a*], Simon Geiger[a], Simon J. Freakley[b], Andrea Mingers[a], Serhiy Cherevko[a,c], Graham J. Hutchings[b], Karl J. J. Mayrhofer[a,c,d*]

[a]*Department of Interface Chemistry and Surface Engineering, Max-Planck-Institut für Eisenforschung GmbH, Max-Planck-Strasse 1, 40237 Düsseldorf, Germany*

[b]*Cardiff Catalysis Institute, School of Chemistry, Cardiff University, Main Building, Park Place, Cardiff, CF10 3AT*

[c]*Helmholtz-Institute Erlangen-Nürnberg for Renewable Energy (IEK-11), Forschungszentrum Jülich, Egerlandstr. 3, 91058 Erlangen, Germany*

[d]*Department of Chemical and Biological Engineering, Friedrich-Alexander-Universität Erlangen-Nürnberg, Egerlandstr. 3, 91058 Erlangen, Germany*

[*]*Corresponding authors: pizzutilo@mpie.de mayrhofer@mpie.de*

*Tel.: +49 211 6792 160, FAX: +49 211 6792 218*

## Abstract

Palladium (Pd) is considered as a possible candidate as catalyst for proton exchange membrane fuel cells (PEMFCs) due to its high activity and affordable price compared to platinum (Pt). However, the stability of Pd is known to be limited, yet still not fully understood. In this work, Pd dissolution is studied in acidic media using an online inductively coupled plasma mass spectrometry (ICP-MS) in combination with an electrochemical scanning flow cell (SFC). Crucial parameters influencing dissolution like potential scan rate, upper potential limit (UPL) and electrolyte composition are studied on a bulk polycrystalline Pd (poly-Pd). Furthermore, a comparison with a supported high-surface area catalyst is carried out for its potential use in industrial applications. For this aim, a carbon supported Pd nanocatalyst (Pd/C) is synthesized and its performance is compared with that of bulk poly-Pd. Our results evidence that the transient dissolution is promoted by three main contributions (one anodic and two cathodic). At potentials below 1.5 $V_{RHE}$ the anodic dissolution is the dominating mechanism, whereas at higher potentials the cathodic mechanisms prevail. On the basis of the obtained results, a model is thereafter proposed to explain the transient Pd dissolution.



Keywords: palladium, dissolution, ORR catalyst, ICP-MS, PEMFC


## 1 Introduction

Pd is a commonly used transition metal that exhibits high catalytic activity towards several electrochemical processes, such as formic acid oxidation [1-3], alcohols oxidation [4-6], hydrogen evolution/oxidation reactions (HER/HOR) [7-9] and oxygen reduction reaction (ORR) [2, 7, 10-12]. Therefore, it is an interesting

candidate for low temperature fuel cells both in alkaline (alkaline fuel cell, AFC) and acidic media (polymer electrolyte membrane based fuel cells, PEMFCs) [13]. Particularly PEMFCs are considered nowadays as attractive and efficient energy-conversion devices for emission-free stationary and mobile applications, which may play a primary role in the future of sustainable energy solutions [14]. However, crucial issues like the high costs and rarity of catalysts for the sluggish oxygen reduction reaction (ORR), for which platinum (Pt) represents the state of the art catalyst, delay the commercialization on a large scale [15-17]. Great efforts have been recently made to reduce the amount of Pt (i.e. via alloying) or to replace it with less costly and/or more abundant non-Pt-based material [18, 19]. Pd along with Pt, stands out as the metal with the smallest overpotential, i.e. highest activity, for the ORR [20]. Indeed, while slightly less active than Pt [7, 21], the costs are around 50% lower than for Pt [10]. Furthermore, binary Pd-M (M=Cu, Co, Ni, Fe) and ternary alloys showed higher activities compared to pure Pt [12, 22-27].

Beside activity, catalyst stability is essential to meet industrial and economical requirements. Metal dissolution (along with the eventual successive re-deposition) was demonstrated to be of primary importance in the course of PEMFC catalyst degradation[28]. Yet, the mechanisms of noble metal dissolution processes are still largely unknown, and contradictory results on the amount of dissolved metal under various operation conditions and on the exact metal dissolution onset potentials are often reported [29, 30].

The Pourbaix diagram suggests that Pd can be thermodynamically oxidized and even dissolved at pH values and potentials relevant for PEMFCs[31]. However, despite the similarity with Pt, Pd exhibits important differences in its electrochemical behavior.

Indeed, at high anodic potentials it is more prone to the formation of higher oxides (i.e. $PdO_2$), hydrous oxide growth and oxygen absorption into the outer layers of the Pd lattice, thus resulting in a higher dissolution rate compared to Pt [32, 33].

The nature of the oxide species formed on the Pd surface and the relation to its dissolution are still under debate [30]. Contradictory results are also reported on the Pd dissolution mechanism. Rand and Woods, studying the dissolution by cyclic voltammetry and calculating the difference between the charge associated with anodic oxidation and cathodic reduction, firstly concluded that Pd dissolution is mainly an anodic mechanism [33], which was successively supported by other authors [34, 35]. Vracar *et al.* proposed that the anodic dissolution is determined by the transfer of a second electron to Pd(OH) species yielding $PdO/Pd(OH)_2$ [36]. Many authors, argue instead that the Pd electrodissolution is mainly a consequence of reduction of Pd oxides [30], such as Pd(OH) [34, 37-39], PdO and $PdO_2$ [30, 37, 40-44], thus resulting in a dominant cathodic process. The electrodissolution of Pd is influenced by several factors, including: (i) nature of anions and cations [30, 45, 46], (ii) H absorption accompanied with formation of α and β hydrides [47, 48], (iii) pH and the electrolyte concentration [30, 49, 50], (iv) high temperature by influencing the solubility product [33], (v) scan rate, applied potential protocol [30, 50] and surface morphology/composition [50].

While most of these studies suggest Pd dissolution under potential cycling, only few works report time-resolved data on dissolution of Pd, which can provide a better insight on the dissolution mechanisms by relating the dissolution rates with the surface oxidation state. Cadle [44] and Bolzàn *et al.* [34] used a rotating ring disk electrode (RRDE) to collect the dissolved Pd species ($Pd^{2+}$ was suggested), thus they were the first to study the time-resolved anodic and cathodic Pd dissolution in

sulfuric acid. Recently, Shrestha *et al.* [43] used a channel flow double electrode (CFDE) to study Pd dissolution. CFDE is in principle similar to RRDE: gold collectors in a flow configuration follow a Pd working electrode. Their system is efficacious in relating the surface transitions with the dissolution in a time-resolved manner; however, the direct quantitative measurement of the dissolved mass was not done. Furthermore, studies at high potentials, where higher oxidation states might occur, are challenging since the oxygen evolved at the working electrode causes a high reduction current at the working electrode [43], thus masking the contribution of dissolution. The use of a quartz crystal microbalance is also a useful approach to relate online surface processes like also Pd dissolution in a quantitative way as shown by Grdeń *et al.* and Łukaszewski *et al.* [51, 52]. Nevertheless, a study of the dissolution also in the oxygen evolution potential region has not been done despite its fundamental interest, as it is known that these two processes are closely related [53]. Additionally, the vast majority of these works only deal with bulk Pd, whereas the stability of high-surface-area catalysts used in real applications has not been studied thoroughly so far [54, 55].

In recent years, the implementation of an electrochemical scanning flow cell (SFC) combined with time-resolved monitoring of the dissolved species present in the electrolyte by using an on-line inductively coupled plasma mass spectrometer (ICP-MS) provided new insights on the dissolution of noble metals like Pt [56, 57] and Au [58, 59]. Nevertheless, even if perceived to be of paramount importance [43], a detailed study of the dissolution mechanism of Pd and the influence of the applied operational conditions has not been done with this technique yet.

In this context, we present here a first investigation on Pd dissolution with the coupled SFC/ICP-MS approach. In particular, we analyze the influence of fundamental parameters such as the upper potential limit (UPL), the scan rate and the anions in commonly used acid electrolytes (sulfuric and perchloric) on the dissolution process. Additionally, we compare the dissolution of bulk poly-Pd with a supported Pd/C catalyst, to validate the results for high-surface area catalysts. Based on the experimental outcome of this comprehensive study we suggest a mechanism for Pd dissolution, even though the exact chemistry of the Pd oxidation is not yet completely resolved.

## 2 Experimental

### 2.1 Nanoparticles synthesis, characterization

The carbon supported Pd was prepared via a colloidal immobilization method described in a previous publication [60]. Initially, the desired amount of a $PdCl_2$ aqueous solution (from Johnson Matthey) was used to prepare a Pd colloidal suspension. Separately, an aqueous solution of $NaBH_4$ (0.1 M) and Poly(vinyl alcohol) (PVA) (1 wt% aqueous solution, Aldrich, MW=10 000, 80% hydrolyzed) were prepared as well, and a precise amount of which was then mixed with the $PdCl_2$ solution: for the PVA solution (1 wt%) was needed (PVA/(Pd) (w/w)=1.2), whereas for the $NaBH_4$ solution (0.1 M, $NaBH_4$/(Pd) (mol/mol)=5) was added. After 30 min, a dark-brown sol is generated. To immobilize the formed colloid an activated carbon (XC72R Vulcan carbon) was added to the colloidal solution and acidified at pH 1 by sulfuric acid (the amount of carbon was calculated to yield a final 10 wt% of final metal/carbon loading). After 2 h of vigorous stirring, the slurry was filtered and

144 washed with distilled water thoroughly. Finally, the catalyst was dried at 120 C for
145 16 h obtaining a dry catalyst powder.

146 The synthesized Pd/C powder was thereafter dispersed in ultrapure water (UPW,
147 PureLab Plus system, Elga, 18 MΩ·cm) obtaining a black homogeneous ink suspension
148 that was easily printed into glassy carbon (GC) plates or RDE tip. Prior to any
149 electrochemical measurement, a small droplet of ink was deposited onto a TEM grid
150 (lacey carbon film supported by a gold grip from Plano GmbH) and examined by
151 transmission electron microscopy (TEM, JEOL JEM-2200FS operated at 200 kV in
152 STEM mode). From the bright field TEM micrograph obtained, the particle size
153 distribution was determined.

154 **2.2 Electrode preparation**

155 Before each experiment, the poly-Pd disk electrode was polished thoroughly with 0.3
156 and 1 μm alumina on a polishing cloth (Strueurs, MD Mol), followed by washing in
157 ultrapure water and drying in argon, obtaining a shiny Pd surface.

158 To prepare the high-surface-area Pd/C electrodes the catalyst ink was printed onto
159 freshly mirror-polished GC plates by mean of a drop-on-demand printer (Nano-
160 PlotterTM 2.0, GeSim). The Nano-Plotter allows the printing in rapid succession of
161 catalyst layers using a piezoelectric pipette. Each layer consisted of 100 drops whose
162 volume was estimated during the measurement (250 pL) and it consist of a circular
163 deposits of a Pd/C catalyst. Two layers were used for all experiments corresponding
164 to approximately 5 ng of metal.

165 **2.3 Electrochemical characterization**

166 The majority of the results on the Pd electrochemical dissolution experiments were
167 obtained using a scanning flow cell (SFC) described in our previous works [57, 58].

168 The electrolytes employed were gas (Ar) purged 0.1 M $H_2SO_4$ and 0.1 M $HClO_4$. These
169 were prepared from concentrated acid (Suprapur®, Merck) diluted in UPW (PureLab
170 Plus system, Elga, 18 MΩ·cm). A poly-Pd disk (5 mm diameter from MaTeck) and the
171 synthesized Pd/C catalyst deposited onto the GC plate were used as working
172 electrodes (WE). The aperture of the SFC cell is 0.01 $cm^2$, slightly larger than the size
173 of the printed spots, thus the SFC was approached easily to the single spot.
174 Dissolution results for poly-Pd in the two considered electrolytes are normalized with
175 the geometrical surface area ($S_{geo}$ in $cm_{geo}^{-2}$). For the comparison between poly-Pd
176 and Pd/C, instead, dissolution is normalized to the real surface area ($S_{real}$ in $cm_{real}^{-2}$).
177 The $S_{real}$ is obtained using the Pd-oxide reduction charge of the last activation CV with
178 an UPL of 1.4 $V_{RHE}$ with the surface charge of 424 μC $cm^{-2}$ [30]. The three-electrode
179 configuration was completed with a graphite rod as counter electrode and an Ag/AgCl
180 as reference electrode. A LabVIEW-based, in-house developed, software controlled
181 the potentiostat (Gamry Reference 600, USA) and all experimental parameters. The
182 chosen electrolyte was flowing through the SFC (flow rate of 180 μL $min^{-1}$) and then
183 downstream to an inductively-coupled plasma mass spectrometer (ICP-MS, NexION
184 300X, Perkin Elmer) where the dissolved element is detected. The quantitative
185 evaluation of the dissolved $^{106}Pd$ was achieved using as internal standard $^{103}Rh$.

186 The poly-Pd cyclic voltammogramms in the two electrolytes were also studied with a
187 rotating disk electrode (RDE) method, for an initial comparison to validate the SFC
188 system. A in-house-built three electrode electrochemical cell with separate
189 compartment made of Teflon® was employed (for details see ref. [61]). The working
190 electrode was a Pd disk of 5 mm diameter (from MaTeck), whereas, as for the SFC,
191 graphite rod and an Ag/AgCl were used as counter and reference electrode,
192 respectively.

193 The experiments were carried out only at room temperature (≈24°C) and all the
194 potentials reported in this work are referred to the reversible hydrogen electrode
195 (RHE), which was measured prior to each single experiment.

196

197 **3 Results**

198 **3.1 Oxidation and reduction of poly-Pd in acidic media**

199

200 Pd cyclic voltammogramms in deaerated solution (Figure 1) are recorded using the
201 SFC with perchloric and sulfuric acid as electrolytes. The curves show typical profiles
202 for a poly-Pd electrode in the aqueous acidic solutions. The Pd electro-oxidation in
203 0.1M $HClO_4$ commences in the anodic scan at approximately 0.7 $V_{RHE}$ ($A_1$ peak). A
204 well-defined oxide reduction peak with a maximum around 0.64 $V_{RHE}$ is visible below
205 0.8 $V_{RHE}$ ($C_1$ peak) in the cathodic scan direction, in agreement with other works [30,
206 48, 62, 63]. Typically a second poorly defined peak for oxide-reduction around 1.2-1.3
207 $V_{RHE}$ is reported in literature (here, $C_2$ peak), which is thought to correspond to the
208 reduction of Pd(IV)-oxide formed at high potentials [30, 63]. In the CVs in Figure this
209 broad peak, though labelled, is not visible due to the low upper potential limit (UPL)
210 applied. However, it will be important in the following sections, where the dissolution
211 at higher UPLs (up to 1.8 $V_{RHE}$) is presented and discussed.

212 Interestingly the CVs show a distinct difference in the Pd oxidation/reduction in the
213 two different electrolytes. Indeed, the onset potential for the electro-oxidation of Pd
214 in sulfuric acid (ca. 0.75 $V_{RHE}$) is slightly shifted compared to perchloric acid (Figure
215 1). This is consistent with the difference in anion adsorption strength, which is known
216 to influence the Pd electro-oxidation [30]. According to Solomun, perchlorate anions

($ClO_4^-$) do not undergo specific adsorption so that only weak (electrostatic) interactions occur between the anions of the electrolyte and the Pd electrode surface, while the interaction of other anions such as the (bi-)sulfate anion ($HSO_4^-/SO_4^{2-}$) is stronger [40-42]. Furthermore, in sulfuric acid, the Pd reduction peak is slightly shifted to higher anodic potentials (0.67 $V_{RHE}$) and the associated charge is slightly higher. A more detailed discussion on Pd oxidation will be provided in the final part of the present work and the interested reader is also referred to the critical review on Pd literature of Grdeń et al. [30].

Pd voltammograms with a lower potential limit (LPL) of 0.05 $V_{RHE}$ are also recorded in an SFC and compared with RDE measurements to validate the results (SI). At low potentials (E<0.3 $V_{RHE}$) a large cathodic current originates from the concurrent H adsorption and bulk absorption, with the formation of Pd hydride. Indeed, unlike Pt, Pd absorbs hydrogen in a potential range where the under potential deposition of H ($H_{UPD}$) as well as the hydrogen evolution (HER) occurs [30, 64]. At higher potentials than HER, the desorption of the absorbed hydrogen ($H_{abs}$) in the poly-Pd bulk structure takes place. This results in a large anodic current, which overlaps with other anodic processes at the surface.

### 3.2 Poly-Pd electrodissolution in different acidic media: influence of UPL

Potential sweeps to increasing upper potential limits (UPL) in two different acidic media (perchloric and sulfuric acid) are applied to poly-Pd electrode. The potential program and the corresponding dissolution profile are presented in Figure 2 a-b, respectively.

The cleaning cycles (30 CVs at 200 mV $s^{-1}$) are characterized by an initially higher Pd dissolution signal, which is probably due to the contribution of initially present

surface defects. After approximately 10 CVs a constant Pd dissolution signal and a stable CV is measured, indicating that a clean, steady surface state for this potential window is obtained.

During the slow potential cycling (10 mV $s^{-1}$), Pd dissolution is observed at potentials where Pd oxidizes (E > 0.7 $V_{RHE}$) and a small deviation from the background signal is observable first with an UPL above 0.8-0.85 $V_{RHE}$, in line with the onset potential shown by Łukaszewski *et al.* obtained with the quartz microbalance [52]. The amount of formed Pd oxide and thus the dissolution increase with the applied UPL. In fact, the charge associated to the reduction peaks increases gradually with potential (Figure 2 c-d and SI). Furthermore, the hysteresis between anodic and cathodic scan increases as the $C_1$ reduction peak shifts to lower potentials. A similar behavior was observed also for Pt [57], and its origin is not fully understood at present [30]. At different UPL up to three different peaks in the Pd dissolution profile (corresponding to the peak anodic $A_1$ and cathodic $C_2$, $C_1$ respectively) can be observed. A comparison of the mass dissolved during the anodic and the two cathodic contributions to the transient dissolutions in the two acids are shown in Figure 3.

The cathodic dissolution peaks ($C_2$ and $C_1$) increase constantly (Figure 3 a-b) with increasing UPL as more oxide is formed, with $C_2$ becoming the dominating contribution at high potential. Instead, the anodic contribution ($A_1$) to the transient dissolution behaves differently (Figure 3 c). Indeed, it is possible to identify different stages in the anodic transient dissolution behavior: (i) A first immune region at potentials lower than Pd oxidation; (ii) a region between 0.8 and 1.4 $V_{RHE}$ where the transient anodic dissolution is increasing with the UPL; (iii) a region in the 1.4-1.7 $V_{RHE}$ potential range, where the transient anodic dissolution is constant

(independently of the UPL), due probably to the oxide coverage that lead to passivation and (iv) a region for potential higher than 1.7-1.8 $V_{RHE}$, where the transient anodic dissolution increases again and could be attributed to the surface change in the OER potentials. Anodic passivation is also confirmed by the decay in the dissolution signal during potentiostatic (steady-state) experiment (SI).

The quantitative total dissolution of Pd per cycle is reported in Table 1, along with the measured dissolution of Pt and Au under similar conditions. Comparing the dissolution in the same medium (sulfuric acid), it turns out that Pd is dissolving at a much higher rate than the other noble metals considered. Furthermore, Pd in sulfuric acid dissolves 5 times more than in perchloric acid. Similar trends were reported in other works [30, 33, 52] and it was attributed to the formation of different complexes between the dissolved species and the anion in the electrolyte (see discussion).

**Table 1 Comparison of the amount of Au, Pt [58], Pd in 0.1M $H_2SO_4$ and Pd* in 0.1M $HClO_4$ dissolved per cycle depending on the applied UPL as derived from potential sweep experiments at 10 mV $s^{-1}$. BDL stands for below the detection limit.**

| UPL / $V_{RHE}$ | Au / ng $cm_{geo}^{-2}$ $cycle^{-1}$ | Pt / ng $cm_{geo}^{-2}$ $cycle^{-1}$ | Pd / ng $cm_{geo}^{-2}$ $cycle^{-1}$ | Pd* / ng $cm_{geo}^{-2}$ $cycle^{-1}$ |
|---|---|---|---|---|
| 0.9 | BDL | BDL | 0.36 | 0.02 |
| 1.0 | BDL | BDL | 5.1 | 0.8 |
| 1.1 | BDL | 0.4 | 21.3 | 4.8 |
| 1.2 | BDL | 1.3 | 51.5 | 12.9 |
| 1.3 | BDL | 2.7 | 83.6 | 18.9 |
| 1.4 | 1.6 | 4.4 | 114.2 | 22.3 |

| | | | | |
|---|---|---|---|---|
| 1.5 | 4.4 | 5.8 | 149.9 | 26.6 |
| 1.6 | 7.4 | 7.0 | 185.8 | 32 |
| 1.7 | 12.5 | 8.0 | 224.4 | 39 |
| 1.8 | 20 | 9.0 | 271.7 | 50 |

Note that until 1.1 $V_{RHE}$ only a single dissolution peak is visible in both electrolytes, while at more positive potentials two to three peaks are observed. However, the applied scan rate (10 mV $s^{-1}$) does not allow a clear separation between the individual dissolution peaks. Therefore, some measurements at selected UPLs with a slower scan rate (2 mV $s^{-1}$) are presented in the next paragraph.

### 3.3 Poly-Pd electrodissolution in different acidic media: slower scan rate

Potential sweeps to increasing UPL (0.9, 1.2, 1.5, 1.8 $V_{RHE}$) in the two different acidic media (perchloric and sulfuric acid) with a 2 mV $s^{-1}$ scan rate are applied to a poly-Pd electrode (Figure 4 a-b). At this slow scan rate the different dissolution processes occurring during cyclic voltammetry can be clearly distinguished. As expected, due to the slower scan rate, the dissolution per cycle is higher; furthermore, the observed quantitative difference between dissolution in perchloric and sulfuric acid is confirmed (see values in SI).

Colored arrows mark the positions of the peaks: red corresponding to the anodic oxidation/dissolution ($A_1$), grey and blue corresponding to the two cathodic reduction/dissolution peaks ($C_2$ and $C_1$ respectively). For the sake of clarity, the single dissolution profiles are shown separately in SI.

The UPLs are chosen in order to distinguish dissolution processes occurring at different potentials. (i) At a potential lower than 1.1 $V_{RHE}$ only one peak is present as a

combined minor anodic and cathodic peak. (ii) In the potential range between 1.1 and 1.4 $V_{RHE}$ a shoulder peak related to the cathodic dissolution due to the $C_1$ reduction starts to appear (blue arrow). With the measured UPL of 1.2 $V_{RHE}$ the maximum of this second peak is measured at 0.8 $V_{RHE}$ during the cathodic scan, which well corresponds to the $C_1$ peak observed in CV with the same UPL. (iii) At more positive potentials a third dissolution peak between the two is appearing (gray arrow) and is increasing dramatically. With an UPL of 1.5 $V_{RHE}$ the maximum of this third peak is measured at 1.1-1.2 $V_{RHE}$ during the cathodic scan, which matches the broad reduction peak $C_2$ observed in the CVs.

The mass cyclic voltammograms of these 4 CVs in perchloric and sulfuric acid are shown in Figure 4 c-d, indicating the trend of the three different contributions (one anodic and two cathodic) to the dissolution more clearly. At potentials up to 1.5 $V_{RHE}$ the three peaks are not perfectly separated, despite the very low scan rate (2 mV $s^{-1}$), while at 1.8 $V_{RHE}$ the anodic dissolution and the first cathodic dissolution peaks appear nicely distinguished. Furthermore, the anodic dissolution maxima appear to be at the same potential for all the four cycles, whereas the cathodic dissolution maxima shift to lower potentials in accordance with the shifts of the reduction peaks (Figure 2 c-d). These shifts are attributed to the irreversibility of the oxide formation [30] and are reported also for other noble metals [57, 65]. Interestingly, in sulfuric acid the dissolution maximum appears to be before the reduction maximum (the former is approximately 30 mV higher; see SI). Similar findings were also obtained for Pt cathodic dissolution in sulfuric acid [66]. In perchloric acid, instead, the two peak potentials correspond well. This difference is not well understood at present and it might derive from the different interactions of the electrolyte anion with Pd. Along

with the change in the maxima, also the cathodic dissolution onset potentials are shifting to lower potentials with increasing UPL.

These results allow us already to dissipate some controversy about the nature of Pd dissolution. As discussed in the introduction, there is an ongoing debate whether Pd dissolution is an anodic process or not. The relative contribution to the dissolution of the three different peaks is shown in the inlet of Figure 4 c-d. At low UPL the process is predominantly anodic (note that however below 1.1 $V_{RHE}$ only one peak is appearing and is not possible to distinguish between anodic and cathodic dissolution). Increasing the UPL it first appear the peak $C_1$ and above 1.4 $V_{RHE}$ the peak $C_2$. In perchloric acid with an UPL of 1.8 $V_{RHE}$ the anodic contribution is reduced to around 37% ($A_1$) and the cathodic rises up to 63% (52 and 11% for $C_2$ and $C_1$ respectively). Thus, with increasing UPL the transient dissolution of Pd switches from an anodic process to a process dominated by Pd-oxide reduction. Moreover, at potentials where the OER becomes relevant the $C_2$ reduction/dissolution process becomes dominant.

### 3.4 Comparison of poly-Pd and Pd/C electrodissolution

In order to estimate the value of the previous results obtained on poly-Pd for real application, carbon supported Pd nanoparticles (Pd/C) are synthesized and analyzed. Firstly, representative bright field TEM micrographs are acquired and the statistical size distribution is evaluated (Figure 5 a). The average particle size is ca. 4.0 nm, which corresponds to an electrocatalytic surface area (ECSA) of 124 $m^2\ g^{-1}$ (see SI for calculation). The synthesized Pd/C catalyst powder is dispersed through sonication in

348 ultrapure water (UPW) and the prepared ink is printed on a glassy carbon (GC) plate
349 obtaining spots that are measured using the SFC.

The Pd/C dissolution measurement (Figure 5 b-c) follows the same protocol reported in Figure 4 and is performed only in perchloric acid with two printed catalyst layers (ca. 5 ng). This corresponds to an initial Pd/C catalyst surface area of 0.0062 $cm^2$ (estimated from the TEM size distribution and the loading in SI). Electrochemical evaluation from the Pd-oxide reduction charge of the first CV [0.1-1.4 $V_{RHE}$] of freshly prepared Pd/C electrode, yields a surface area of 0.0054 $cm^{-2}$ (see SI). The electrochemical determination of the surface area through Pd-oxide reduction is convenient but not straightforward as it requires a precise knowledge of the potential formation of 1 oxide monolayer (ML). In the literature, this is indicated to be for polycrystalline Pd in the range 1.4-1.5 $V_{RHE}$, even though lower values are also reported [30, 67]. To compare the electrochemical dissolution of two different systems like bulk and nanoparticulate Pd, the dissolution data shown in Figure 5 b-c are normalized by the real surface area ($S_{real}$), which is 0.0109 and 0.0035 $cm^{-2}$ for poly-Pd and Pd/C respectively. This is determined from the Pd-oxide reduction of the last activation cycle ([0.1-1.4] $V_{RHE}$), which directly precede the dissolution measurement. Pd-oxide reduction and thus $S_{real}$ during activation of Pd/C decrease by ca. 35% indicating a surface area change due to catalyst degradation. At low potentials, the poly-Pd and Pd/C CVs show one interesting difference between catalysts: unlike poly-Pd, Pd/C does not show a large cathodic current and anodic peak corresponding to the H bulk absorption (inlet in Figure 5 b). This behavior was already known in literature and was reported to be size dependent [68, 69].

Potential sweeps to increasing UPL (0.9, 1.2, 1.5 $V_{RHE}$) in perchloric acid with a 2 mV $s^{-1}$ scan rate are applied to poly-Pd and Pd/C (Figure 5 b-c). The same feature for poly-Pd, namely the presence of up to three peaks in the dissolution profile are also observed for Pd/C. While the anodic peak $A_1$ and cathodic peak $C_2$ well correspond,

375 the cathodic dissolution $C_1$ is shifted for Pd/C to lower potentials (time delay in
376 Figure 5 c). The peak position generally depends on different parameters such as the
377 mass transfer of dissolved species out of the carbon matrix, the flow rate and scan
378 rate. While the last two are the same in both measurements, the amount of printed
379 Pd/C catalyst is so low that the mass transfer limitation can be neglected. A more
380 valuable explanation relates to the shift of the reduction to lower potential for Pd/C
381 (see inlet CVs in Figure 5 b).

382 Considering the quantitative dissolution, it is observed a slightly higher dissolution
383 per electrochemical real surface area in the case of nanoparticulate Pd/C catalyst
384 (Figure 5 c) at all considered potentials. Only few works are reported in the literature
385 of nanoparticulate palladium dissolution and to the knowledge of the author no on-
386 line detection of dissolved Pd from nanoparticles is reported. Generally they indicate
387 influence of surface morphology, geometry and particle sizes [54, 55]. Kumar *et al.*
388 studying the anodic oxidation onset potential in presence of chlorides suggested a
389 size dependent destabilization of the nanoparticles compared to bulk Pd [55]. In our
390 case, we do not see any significant difference in dissolution onset potential between
391 the two electrode systems, but the dissolution profiles suggest a small difference in
392 their behavior. Note however that a precise quantitative evaluation is rather
393 challenging especially when dealing with nanoparticulate catalyst. Indeed, (i) the $S_{real}$
394 is determined with the same electrochemical method for both catalyst even though
395 the precise potential of formation of 1 oxide ML can slightly change with surface
396 morphology and geometry. Indeed, with same UPL the oxide formation and reduction
397 might be different from nanoparticles and bulk Pd [55]. Furthermore, (ii) $S_{real}$ of Pd/C
398 might change during measurement in consequence of dissolution and catalyst
399 degradation (even though measurements are limited to 3 cycles to minimize

degradation). Furthermore, (iii) remaining PVA from synthesis might influence the dissolution (even though the washing step is expected to remove it). Finally, (iv) for carbon supported nanoparticles the catalyst loading in the experiment might also play a role as shown recently by Keeley *et al.* [29]. Indeed, the authors showed for Pt/C that the specific dissolution (normalized per surface area) is decreasing when the loading increases. This phenomenon was attributed to the decreased diffusion of Pt ions into bulk solution as ions remain trapped in the porous catalyst deposit when loading is higher.

## 4 Discussion

The major experimental findings of this work can be summarized as follow:

(i) The Pd dissolution is strictly correlated to the oxide formation and reduction. However, no simple correlation could be established between the two processes. Indeed, the dissolution onset potential in perchloric acid appears to be around 50 mV higher than in sulfuric acid, whereas the oxidation onset potential in perchloric acid is slightly lower (Figure 1);

(ii) Below 1.1 $V_{RHE}$ it was not possible to differentiate between anodic and cathodic processes. Between 1.1 and 1.4 $V_{RHE}$ a cathodic dissolution related to the $C_1$ reduction is observed. At more positive potentials a third dissolution peak, corresponding to the broad $C_2$ reduction, appears and it increases dramatically with the UPL (Figure 2-4).

(iii) Increasing the UPL, the oxide coverage increases. Therefore, while transient anodic dissolution initially increases with UPL, in the 1.4-1.7 $V_{RHE}$ potential range the formed oxide protects Pd from increasing dissolution.

Beyond 1.7-1.8 $V_{RHE}$ anodic dissolution increases again in correspondence to the OER region (Figure 3);

(iv) Unlike for anodic dissolution the cathodic dissolution increases almost linearly with UPL (Figure 3), becoming the dominant process for potential higher than 1.7 $V_{RHE}$. Furthermore, its onset and maxima shifts to lower potentials with increasing UPL (Figure 4), in accordance with the shift of the cathodic $C_1$ and $C_2$ reduction peaks (Figure 2);

(v) Pd dissolves much more than Pt and Au and the dissolution depends strongly on the scan rate. Pd dissolution in sulfuric acid was found to be 5 times higher than in perchloric acid (Table 1);

(vi) In potentiostatic experiments below 1.6 $V_{RHE}$ the dissolution rate decreases with time, indicating the passivation of the surface (SI);

(vii) All these findings were additionally validated for a carbon supported high-surface area Pd/C nanocatalyst, which is more interesting for application. A slightly small increase in dissolution per real surface are is observed for Pd/C (Figure 5).

With our findings we confirmed the close connection between the Pd oxidation states and its transient dissolution, which was already observed for Au and Pt electrode materials [59]. Indeed, the electrochemical oxidation and the dissolution of Pd have similar standard potentials. Pourbaix expressed the oxidation of Pd as [31]:

$$Pd + H_2O \rightarrow PdO + 2H^+ + 2e^- \quad \textbf{(1)}$$

$$E^o = 0.917 + 0.0591\log[H^+]$$

or $$Pd + 2H_2O \rightarrow Pd(OH)_2 + 2H^+ + 2e^- \quad \textbf{(1b)}$$

$$E^o = 0.897 + 0.0591\log[H^+]$$

$$PdO + H_2O \rightarrow PdO_2 + 2H^+ + 2e^- \quad \textbf{(2)}$$

$$E^o = 1.263 + 0.0591\log[H^+]$$

or $$Pd(OH)_2 + 2H_2O \rightarrow Pd(OH)_4 + 2H^+ + 2e^- \quad \textbf{(2b)}$$

$$E^o = 1.283 + 0.0591\log[H^+]$$

444

445 And the dissolution of Pd can be described as [31]:

$$Pd \rightarrow Pd^{2+} + 2e^- \quad \textbf{(3)}$$

$$E^o = 0.987 + 0.0295\log[Pd^{2+}]$$

$$PdO_2 + 4H^+ + 2e^- \rightarrow Pd^{2+} + H_2O \quad \textbf{(4)}$$

$$E^o = 1.194 + 0.1182\log[H^+] - 0.0295[Pd^{2+}]$$

$$PdO + 2H^+ \rightarrow Pd^{2+} + H_2O \quad \textbf{(5)}$$

$$\log[Pd^{2+}] = -3.02 + 2\log[H^+]$$

or $$Pd(OH)_2 + 2H^+ \rightarrow Pd^{2+} + 2H_2O \quad \textbf{(5b)}$$

$$\log[Pd^{2+}] = -2.35 + 2\log[H^+]$$

446

447 As anticipated, despite the large amount of literature and the variety of methods
448 applied, several aspects of Pd electro-oxidation are still poorly understood, such as

449 the chemical composition, thickness and adsorption behavior of Pd oxide layers [30].
450 In particular, there are some relevant issues in the literature that require additional
451 research [30]: (i) the first product formed during oxidation was considered by several
452 authors to be Pd($OH_{ads}$) [34, 38, 39, 48, 63, 70], while other authors suggested the
453 formation of Pd(II)-oxide/hydroxide species such as PdO [30, 71] or $Pd(OH)_2$ [31]; (ii)
454 the potential for the formation of an oxide monolayer (generally reported to occur
455 around 1.45-1.5 $V_{RHE}$) is unclear, as is (iii) the onset potential for the formation of
456 higher oxidation species (i.e Pd(IV)-oxide, thicker β Pd(IV)-oxide in the OER region);
457 (iv) the presence of subsurface oxygen is claimed by some groups to play an
458 important role in the reactivity and stability of the metal [32, 41, 72] and (vi) it is not
459 obvious if anhydrous/hydrous oxide is present or not at different potentials.
460 Concerning the last point, we will consider both reactions (equations 1-1b and 2-2b),
461 but in the following discussion we will rather talk of Pd(II)- and Pd(IV)-oxides.

462 In the literature two Pd reduction peaks are reported: (i) a well-defined reduction
463 peak at lower potentials labeled here as $C_1$ (Figure 1) that corresponds to the
464 reduction of Pd(II)-oxide (equation 1-1b) and (ii) a second broad reduction peak
465 around 1.2-1.3 $V_{RHE}$ (here, $C_2$), which is thought to correspond to the reduction of
466 Pd(IV)-oxide formed at high potentials (>1.3 $V_{RHE}$), slightly below the OER onset [30,
467 63] (equation 2-2b). This higher oxidation state was confirmed with XPS
468 measurement by Chausse et *al.* [73]. Zhang *et al*. and Birrs *et al*. showed
469 independently that a thick Pd "β hydrous oxide" [62, 65, 74] is only formed at very
470 large anodic polarization (higher than the OER onset) and its reduction is correlated
471 to several peaks in the low potential region, around $H_{UPD}$ [30, 32, 65]. In our
472 experimental results no peaks of this kind are observed up to 1.8 $V_{RHE}$, therefore the
473 presence of a thicker hydrous oxide layer (elsewhere referred as β oxide [30]) can be

474 safely excluded from the following considerations, at least for potentials up to 1.7
475 $V_{RHE}$.
476 According to the literature and to cyclic voltammetry one would expect already some
477 Pd dissolution in parallel with the initial Pd oxidation, namely around 0.7 $V_{RHE}$ and
478 0.75 $V_{RHE}$ in perchloric and sulfuric acid respectively (Figure 1). However, a small
479 deviation from the background signal is only observable first with an UPL above 0.8-
480 0.85 $V_{RHE}$, close to the thermodynamically predicted standard potential for Pd metal
481 electro-dissolution ($E^0(Pd/Pd^{2+}) = 0.987\ V + 0.0295 \log(Pd^{2+})$), which assuming a
482 reasonable $Pd^{2+}$ concentration of 1 nmol $dm^{-3}$ would be approximately 0.72 $V_{SHE}$ (0.78
483 $V_{RHE}$ at pH=1). Experimentally, there is a more than 100 mV shift for the dissolution
484 onset in comparison to oxidation. A similar difference was already observed for Pt
485 dissolution and it was tentatively related to the ICP-MS detection limit. Recently, a
486 modified scanning flow cell configuration allowed the accumulation of dissolved Pt.
487 Thus, dissolution was measured also at potential, close to the Pt oxidation onset [56].
488 In the case of Pd this difference could be attributed either to the ICP-MS detection
489 limit (as for Pt) or to the higher standard potential of the Pd electro-dissolution
490 compared to the Pd oxidation. Furthermore, the dissolution onset potential in
491 perchloric acid appeared to be around 50 mV higher than in sulfuric acid. This is
492 somehow contradictory with the oxidation onset potential which in perchloric acid is
493 lower (Figure 1). Therefore, no simple correlation between oxidation and dissolution
494 is established, as previously observed for Au in perchloric and sulfuric acid [75].

495 Interestingly, despite exhibiting similar features, the actual measured Pd dissolution
496 in the two different electrolytes is quantitatively very different. Indeed, Pd in sulfuric
497 acid is dissolving at rates approximately 5 times higher than in perchloric media
498 (Table 1). Furthermore, comparing the dissolution in the same medium (sulfuric

499 acid), it turns out that Pd is dissolving at a much higher rate than other noble metals
500 like Pt and Au. Already Rand and Woods [33] reported Pd dissolution to be
501 approximately 30 times higher than Pt in sulfuric acid, in good agreement to our
502 results. Much higher dissolution of Pd compared to Pt was also observed by
503 Łukaszewski *et al.* [52]. Burke *et al.* [32] affirmed that this marked behavior is related
504 to the ionic radii difference of the respective cations. In fact, the electrostatic field
505 around smaller Pd cations is stronger, which leads to more stable Pd complexes and a
506 stronger solvation shell [30], resulting in the observed enhancement in Pd electro-
507 dissolution. The observed Pd dissolution difference in the two acidic electrolytes
508 could be attributed to a difference in the amount of oxide formed in the considered
509 media. Effectively, the UPL being equal, the measured Pd reduction charge in sulfuric
510 acid (Figure 2 c) is visibly higher than in perchloric (Figure 2 d), suggesting less oxide
511 formation with the latter. However, the difference in the reduction charges is only up
512 to ca. 20% (SI). Therefore, different dissolution behavior could be originated by the
513 different nature of the anions in the electrolyte. In the literature, many works
514 reported enhanced electro-dissolution in presence of chlorides and iodides [30, 37,
515 38], however only few works reported differences between perchloric and sulfuric
516 acid, the latter being the sole choice of electrolyte for most of the experimental
517 studies. Recently, Grdeń *et al*. [30] reviewed several Pd studies and classified anions
518 on the basis of their Pd electro-dissolution promotional effect as follows: $ClO_4^-$ <
519 $HSO_4^-/SO_4^{2-}$ < $Cl^-$ < $I^-$. Anions like $Cl^-$ and $I^-$ form stable Pd-anion complexes that can
520 lead to an increase in dissolution [30]. Solomun, studying the role of anions in $H_2SO_4$
521 and $HClO_4$ with LEED and XPS, suggested that the adsorbed anion can weaken the Pd-
522 Pd surface bonds [30, 42]. They also proposed that the adsorption of $HSO_4^-/SO_4^{2-}$ in
523 the early stages of surface oxidation facilitates the interfacial place exchange [40-42],

thus resulting in enhanced Pd dissolution in the case of $HSO_4^-/SO_4^{2-}$, as confirmed with our experimental findings. Furthermore, the dissolved $Pd^{2+}$ can form in acidic electrolytes stable complexes, that if on the one hand can explain the enhanced electro-dissolution of Pd compared to Au and Pt, on the other hand can be at the origin of the different electro-dissolution in $HClO_4$ and $H_2SO_4$.

Even though the absolute amount of dissolved Pd per cycle is quite different in the two electrolytes (see Table 1), the percentage contribution of the different dissolution peaks follow qualitatively the same trend. (i) Below 1.1 $V_{RHE}$ only one peak is present, as at these low potentials it is not possible to distinguish between anodic and cathodic dissolution. (ii) Between 1.1-1.4 $V_{RHE}$ a dissolution peak corresponding to the cathodic reduction $C_1$ is appearing and becoming more and more important. This dissolution peak is observed in the literature with different techniques as RRDE [34, 44], CFDE [43] and quarzt microbalance [51, 52] referred in the literature to Pd(II)-oxide reduction [30]. However, the Pd(II)-oxide can only undergo chemical dissolution (equations 5-5b), which is generally disregarded for other metals like Pt. The Pd solubility is higher than that of Pt and this could mean that, unlike for Pt, the chemical dissolution might play a role for Pd. Nevertheless, the experimental results indicate an existing correlation between the Pd(II)-oxide reduction ($C_1$) and the dissolution peak, which cannot be easily explained only with chemical dissolution. Therefore, the dissolution has been often attributed to the reduction and desorption of adsorbed oxygen species that causes de-passivation (equation 3). (iii) At 1.4 $V_{RHE}$ a second cathodic dissolution peak corresponding to the broad Pd(IV)-oxide reduction ($C_2$) is observed (equations 2-2b). Even though the integration of such a broad peak is not easy, we can safely say that even at high UPL the amount of Pd(IV)-oxide formed is less than the amount of Pd(II)-oxide formed ($C_2$ reduction charge density is much

549 smaller than $C_1$ reduction charge density as shown in SI). On the other hand, the
550 amount of dissolved Pd related to Pd(IV)-oxide reduction ($C_2$) is much larger than the
551 dissolved Pd related to Pd(II)-oxide reduction ($C_1$) (Figure 3). (iv) Above 1.7 $V_{RHE}$ the
552 cathodic dissolution overall exceeds the anodic dissolution. In particular, at 1.8 $V_{RHE}$
553 the cathodic dissolution associated to the Pd(IV)-oxide reduction ($C_2$) becomes the
554 dominant dissolution mechanism.

555 Interesting is the trend of the transient anodic Pd dissolution with different UPLs as
556 shown in Figure 3, where different potential regions can be observed in the two
557 electrolytes. Above 0.9 $V_{RHE}$ Pd oxidation to Pd(II)-oxide (equations 1-1b) and Pd
558 metal dissolution to $Pd^{2+}$ (equation 3) are proceeding in parallel and upon an increase
559 in UPL the transient anodic dissolution increases. Between 1.4 and 1.7 $V_{RHE}$ no
560 increase in transient anodic dissolution is observed. This can have two reasons: (i)
561 Around 1.3-1.4 $V_{RHE}$ a complete monolayer of Pd(II)-oxide is formed, thus preventing
562 further Pd metallic dissolution (through equation 3). In the literature, different
563 studies generally agree that the complete formation of a monolayer occurs between
564 1.4-1.5 $V_{RHE}$ [30]. However, in this case the chemical dissolution of Pd(II)-oxide
565 (equations 5-5b) would still be present in contrast to the observed passivation.
566 Therefore, either the chemical dissolution can be disregarded (as for Pt), or the
567 passivation arises from (ii) the formation of a top layer of chemically stable Pd(IV)-
568 oxide, which is reported to start, as mentioned above, also around 1.3-1.4 $V_{RHE}$.
569 However, if the Pd(IV)-oxide would cover completely the Pd surface one would
570 expect much higher Pd(IV)-oxide reduction charges (peak $C_2$). Therefore, we suggest
571 that the kinetics of the Pd(II)-oxide chemical dissolution (equations 5-5b) is too slow
572 and the associated dissolution products are below the ICP-MS detection limit. In this
573 sense, the contribution of equations 5-5b is neglected in the following mechanistic

574 discussion and the observed passivation between 1.4 and 1.7 $V_{RHE}$ can be explained
575 with the formation of a complete monolayer of Pd(II)-oxide. At more positive
576 potentials the amount of anodically dissolved Pd increases again. The origin of this
577 behavior is not clear yet and should be further investigated. However, this could be
578 attributed to (i) evolution of oxygen (as observed for different metals [76]) and/or to
579 (ii) changes in the oxide structure from a thin α Pd oxide to a thick, hydrous, porous β
580 Pd oxide [37, 65, 74] and/or to (iii) formation of Pd(VI)-oxides [30, 31]. Indeed, the
581 last two are reported to take place above the OER in acidic media.

582 Even though the precise nature of Pd oxide is still unresolved, we showed that its
583 dissolution process can be safely ascribed to surface processes involving different
584 oxidation states and the changes between them. Additional work needs to be done to
585 describe precisely the transient Pd dissolution. Nevertheless, a tentative mechanism
586 can be derived from our experimental observations (Scheme 1).

587 The main contribution to the **anodic dissolution** (related to oxidation peak $\mathbf{A_1}$)
588 comes from metal Pd dissolution to $Pd^{2+}$ (equation 3)(3), that is proceeding in parallel
589 with surface oxidation to Pd(II)-oxide (equations 1-1b). The formed Pd(II)-oxide can
590 be chemically dissolved (equations 5-5b), yielding other $Pd^{2+}$, however as discussed
591 earlier its contribution is neglected. As the potential increases Pd(II)-oxide oxidizes to
592 Pd (IV)-oxide (equations 2-2b). Pd passivates (geometrically and/or
593 electrochemically) once the first oxide monolayer is formed (no increase in transient
594 anodic dissolution). The formed Pd-oxide film is rather complex and depends strongly
595 on the UPL. Nevertheless, we suggest a possible general composition. For UPLs in the
596 0.7-1.4 $V_{RHE}$ potential range, the formation of more Pd(II)-oxide (equations 1-1b) is
597 favored over the formation of Pd(IV)-oxide and a monolayer Pd(II)-oxide is obtained

around 1.4 $V_{RHE}$. Once the potential is raised above 1.4 $V_{RHE}$ the formation of Pd(IV)-oxide becomes thermodynamically favorable and a layer of surface $Pd_s$(IV)-oxide forms on top.

During the cathodic scan, first the $Pd_s$(IV)-oxide is reduced back to Pd(II) (equations 2-2b) (**$C_2$** reduction peak) or dissolved to $Pd^{2+}$ through the electrochemical reaction (equation 4) yielding the **first cathodic dissolution** peak. This peak is only obtained when the UPL is high enough that $Pd_s$(IV)-oxide is formed (equations 2-2b). Furthermore, (equation 4) is dependent on both the pH and the amount of oxide formed. Thus, it can nicely explain the steep increase with the UPL of the amount of dissolved Pd related to this first cathodic dissolution peak. Indeed, it becomes the dominant dissolution mechanism above 1.7 $V_{RHE}$, where more Pd(IV)-oxide is formed.

A **second cathodic dissolution** (related to the reduction peak **$C_1$**) is observed at lower potentials where Pd(II)-oxide reduction (equation 1-1b) takes place. During transient conditions the mechanism of Pd ions production is not well understood. In many past and recent works, this dissolution was related to Pd(II)-oxide reduction yielding $Pd^{2+}$ [43]. Based on electrochemical equilibria [31] Pd(II)-oxide could dissolve in a chemical reduction, which as discussed earlier can be disregarded. It has been suggested elsewhere for Au and other noble metals that the dissolution during the negative direction scan is due to the de-passivation of the oxide, resulting in the dissolution of the exposed metal ion [59]. Effectively, assuming a reasonable $Pd^{2+}$ concentration of 1 nmol $dm^{-3}$, from the dissolved amount of Pd, the equilibrium potential for the Pd metal electro-oxidation ($E^0(Pd/Pd^{2+})$ = 0.987 V + 0.0295 log($Pd^{2+}$), in equation 3) would be approximately 0.72 $V_{SHE}$ (0.78 $V_{RHE}$). At such

potential of the Pd(II)-oxide would be already partially reduced and thus free Pd metal would be exposed to the electrolyte and be available for dissolution. Still, the estimated equilibrium potential of (equation 3) is higher compared to the lowest potential at which dissolution was detected. This could be simply an effect of (i) mass transport limitation and/or (ii) due to the presence of defects and adatoms formed during the oxide reduction whose equilibrium potential can differs from that of the bulk. As another possible contribution to this second cathodic dissolution peak we suggest that some remaining small amount of bulk $Pd_b$(IV)-oxide embedded in the Pd(II)-oxide layer might play a role. Indeed, when Pd(II)-oxide is reduced back to Pd metal the remaining $Pd_b$(IV)-oxide can dissolve in a non-reversible process through (equation 4). In summary, this second cathodic dissolution peak can be explained by assuming a direct dissolution of the Pd metal and/or a dissolution of a remaining Pd(IV)-oxide. Both explanations well match the correspondence of the Pd(II)-oxide reduction peak $C_1$ and the dissolution measured with ICP-MS.

## 5 Conclusion

In conclusion, despite the uncertainty and complexity of the Pd oxidation states and mechanism, in this work we have proposed a model for the transient Pd dissolution based on our unique experimental results. This model is not only suitable for ideal bulk polycrystalline Pd, but our experimental results confirmed its validity also for supported high-surface-area catalysts, which despite their major interests for application were not studied previously. Therefore, our findings will be of interest for future studies on Pd and Pd-based alloys degradation in real applications.

While the proposed mechanism explains the dissolution trends of the presented results, still some unresolved questions remain open and will need further

investigations. First, the lack of a precise knowledge of the chemical species formed at the Pd surface represents an obstacle for a full understanding of Pd dissolution. Secondly, the role of the transition between thin α oxide and thick β hydrous oxide formed at very high anodic polarization or the formation of Pd(VI) oxide and its relevance for the transpassive region could not be clarified. Finally, the influence of parameters such as temperature, the presence of anions and cations in different electrolytes and the nanoparticle size needs further investigation.

## Acknowledgments

The authors thank the MAXNET Energy for the financial support. E.P acknowledges financial support from the IMPRS-SurMat doctoral program. S.G. acknowledges financial support from BASF.

## References

[1] J.F. Chang, L.G. Feng, C.P. Liu, W. Xing, X.L. Hu, An Effective Pd-Ni2P/C Anode Catalyst for Direct Formic Acid Fuel Cells, Angew Chem Int Edit, 53 (2014) 122-126.
[2] L.Y. Chen, H. Guo, T. Fujita, A. Hirata, W. Zhang, A. Inoue, M.W. Chen, Nanoporous PdNi Bimetallic Catalyst with Enhanced Electrocatalytic Performances for Electro-oxidation and Oxygen Reduction Reactions, Adv Funct Mater, 21 (2011) 4364-4370.
[3] K. Jiang, H.X. Zhang, S.Z. Zou, W.B. Cai, Electrocatalysis of formic acid on palladium and platinum surfaces: from fundamental mechanisms to fuel cell applications, Phys Chem Chem Phys, 16 (2014) 20360-20376.
[4] C. Bianchini, P.K. Shen, Palladium-Based Electrocatalysts for Alcohol Oxidation in Half Cells and in Direct Alcohol Fuel Cells, Chem Rev, 109 (2009) 4183-4206.
[5] W. Pan, X.K. Zhang, H.Y. Ma, J.T. Zhang, Electrochemical synthesis, voltammetric behavior, and electrocatalytic activity of Pd nanoparticles, J Phys Chem C, 112 (2008) 2456-2461.
[6] X. Zhao, M. Yin, L. Ma, L. Liang, C.P. Liu, J.H. Liao, T.H. Lu, W. Xing, Recent advances in catalysts for direct methanol fuel cells, Energ Environ Sci, 4 (2011) 2736-2753.
[7] M. Shao, Palladium-based electrocatalysts for hydrogen oxidation and oxygen reduction reactions, J Power Sources, 196 (2011) 2433-2444.
[8] S.A. Grigoriev, P. Millet, V.N. Fateev, Evaluation of carbon-supported Pt and Pd nanoparticles for the hydrogen evolution reaction in PEM water electrolysers, J Power Sources, 177 (2008) 281-285.

[9] T.G. Kelly, S.T. Hunt, D.V. Esposito, J.G.G. Chen, Monolayer palladium supported on molybdenum and tungsten carbide substrates as low-cost hydrogen evolution reaction (HER) electrocatalysts, Int J Hydrogen Energ, 38 (2013) 5638-5644.
[10] H. Meng, D.R. Zeng, F.Y. Xie, Recent Development of Pd-Based Electrocatalysts for Proton Exchange Membrane Fuel Cells, Catalysts, 5 (2015) 1221-1274.
[11] H. Erikson, A. Sarapuu, K. Tammeveski, J. Solla-Gullon, J.M. Feliu, Enhanced electrocatalytic activity of cubic Pd nanoparticles towards the oxygen reduction reaction in acid media, Electrochem Commun, 13 (2011) 734-737.
[12] W.M. Wang, D. Zheng, C. Du, Z.Q. Zou, X.G. Zhang, B.J. Xia, H. Yang, D.L. Akins, Carbon-supported Pd-Co bimetallic nanoparticles as electrocatalysts for the oxygen reduction reaction, J Power Sources, 167 (2007) 243-249.
[13] E. Antolini, Palladium in fuel cell catalysis, Energ Environ Sci, 2 (2009) 915-931.
[14] B.C.H. Steele, A. Heinzel, Materials for fuel-cell technologies, Nature, 414 (2001) 345-352.
[15] I. Katsounaros, S. Cherevko, A.R. Zeradjanin, K.J.J. Mayrhofer, Oxygen Electrochemistry as a Cornerstone for Sustainable Energy Conversion, Angew Chem Int Edit, 53 (2014) 102-121.
[16] S. Koh, P. Strasser, Electrocatalysis on bimetallic surfaces: Modifying catalytic reactivity for oxygen reduction by voltammetric surface dealloying, J Am Chem Soc, 129 (2007) 12624-+.
[17] V.R. Stamenkovic, B.S. Mun, M. Arenz, K.J.J. Mayrhofer, C.A. Lucas, G.F. Wang, P.N. Ross, N.M. Markovic, Trends in electrocatalysis on extended and nanoscale Pt-bimetallic alloy surfaces, Nat Mater, 6 (2007) 241-247.
[18] C.H. Choi, C. Baldizzone, G. Polymeros, E. Pizzutilo, O. Kasian, A.K. Schuppert, N.R. Sahraie, M.T. Sougrati, K.J.J. Mayrhofer, F. Jaouen, Minimizing Operando Demetallation of Fe-N-C Electrocatalysts in Acidic Medium, Acs Catal, 6 (2016) 3136-3146.
[19] E. Antolini, S.C. Zignani, S.F. Santos, E.R. Gonzalez, Palladium-based electrodes: A way to reduce platinum content in polymer electrolyte membrane fuel cells, Electrochim Acta, 56 (2011) 2299-2305.
[20] J.K. Norskov, J. Rossmeisl, A. Logadottir, L. Lindqvist, J.R. Kitchin, T. Bligaard, H. Jonsson, Origin of the overpotential for oxygen reduction at a fuel-cell cathode, J Phys Chem B, 108 (2004) 17886-17892.
[21] L.M. Vracar, D.B. Sepa, A. Damjanovic, Palladium Electrode in Oxygen-Saturated Aqueous-Solutions - Reduction of Oxygen in the Activation-Controlled Region, J Electrochem Soc, 133 (1986) 1835-1839.
[22] O. Savadogo, K. Lee, K. Oishi, S. Mitsushima, N. Kamiya, K.I. Ota, New palladium alloys catalyst for the oxygen reduction reaction in an acid medium, Electrochem Commun, 6 (2004) 105-109.
[23] M.H. Shao, T. Huang, P. Liu, J. Zhang, K. Sasaki, M.B. Vukmirovic, R.R. Adzic, Palladium monolayer and palladium alloy electrocatalysts for oxygen reduction, Langmuir, 22 (2006) 10409-10415.
[24] J. Zhao, A. Sarkar, A. Manthiram, Synthesis and characterization of Pd-Ni nanoalloy electrocatalysts for oxygen reduction reaction in fuel cells, Electrochim Acta, 55 (2010) 1756-1765.
[25] N.N. Kariuki, X.P. Wang, J.R. Mawdsley, M.S. Ferrandon, S.G. Niyogi, J.T. Vaughey, D.J. Myers, Colloidal Synthesis and Characterization of Carbon-Supported Pd-Cu Nanoparticle Oxygen Reduction Electrocatalysts, Chem Mater, 22 (2010) 4144-4152.
[26] M.H. Shao, K. Sasaki, R.R. Adzic, Pd-Fe nanoparticles as electrocatalysts for oxygen reduction, J Am Chem Soc, 128 (2006) 3526-3527.

[27] V. Raghuveer, P.J. Ferreira, A. Manthiram, Comparison of Pd-Co-Au electrocatalysts prepared by conventional borohydride and microemulsion methods for oxygen reduction in fuel cells, Electrochem Commun, 8 (2006) 807-814.
[28] A.A. Topalov, S. Cherevko, A.R. Zeradjanin, J.C. Meier, I. Katsounaros, K.J.J. Mayrhofer, Towards a comprehensive understanding of platinum dissolution in acidic media, Chem Sci, 5 (2014) 631-638.
[29] G.P. Keeley, S. Cherevko, K.J. Mayrhofer, The Stability Challenge on the Pathway to Low and Ultra- Low Platinum Loading for Oxygen Reduction in Fuel Cells, ChemElectroChem, (2015).
[30] M. Grdeń, M. Łukaszewski, G. Jerkiewicz, A. Czerwiński, Electrochemical behaviour of palladium electrode: Oxidation, electrodissolution and ionic adsorption, Electrochim Acta, 53 (2008) 7583-7598.
[31] M. Pourbaix, Atlas of Electrochemical Equilibria in Aqueous Solutions, 2nd ed., Nat. Assoc. of Corrosion Engineers, Houston, Texas, 1974, Chapter IV, 17.1, 1974.
[32] L.D. Burke, J.K. Casey, An Examination of the Electrochemical-Behavior of Palladium Electrodes in Acid, J Electrochem Soc, 140 (1993) 1284-1291.
[33] D.A.J. Rand, R. Woods, Study of Dissolution of Platinum, Palladium, Rhodium and Gold Electrodes in 1 M Sulfuric-Acid by Cyclic Voltammetry, J Electroanal Chem, 35 (1972) 209-&.
[34] A.E. Bolzan, M.E. Martins, A.J. Arvia, The Electrodissolution of Base Palladium in Relation to the Oxygen Electroadsorption and Electrodesorption in Sulfuric-Acid-Solution, J Electroanal Chem, 172 (1984) 221-233.
[35] K. Juodkazis, J. Juodkazyte, B. Sebeka, G. Stalnionis, A. Lukinskas, Anodic dissolution of palladium in sulfuric acid: An electrochemical quartz crystal microbalance study, Russ J Electrochem+, 39 (2003) 954-959.
[36] L.M. Vracar, D.B. Sepa, A. Damjanovic, Palladium Electrode in Oxygen Saturated Solutions - Rest Potentials in Solutions of Different Ph, J Electrochem Soc, 134 (1987) 1695-1697.
[37] A.E. Bolzan, A.J. Arvia, The Electrochemical-Behavior of Hydrous Palladium Oxide Layers Formed at High Positive Potentials in Different Electrolyte-Solutions, J Electroanal Chem, 322 (1992) 247-265.
[38] A.E. Bolzan, A.J. Arvia, Effect of the Electrolyte-Composition on the Electroreduction of Palladium Oxide-Films, J Electroanal Chem, 354 (1993) 243-253.
[39] C.L. Perdriel, E. Custidiano, A.J. Arvia, Modifications of Palladium Electrode Surfaces Produced by Periodic Potential Treatments, J Electroanal Chem, 246 (1988) 165-180.
[40] T. Solomun, Initial-Stages of Electrooxidation of Pd (100) Surfaces in Sulfuric-Acid-Solution - an Xps Study, J Electroanal Chem, 217 (1987) 435-441.
[41] T. Solomun, Electro-Oxidation of the Pd(100) Surface - Potential Dependence of Oxygen Incorporation into the Substrate, J Electroanal Chem, 255 (1988) 163-177.
[42] T. Solomun, The Role of the Electrolyte Anion in Anodic-Dissolution of the Pd(100) Surface, J Electroanal Chem, 302 (1991) 31-46.
[43] B.R. Shrestha, A. Nishikata, T. Tsuru, Channel flow double electrode study on palladium dissolution during potential cycling in sulfuric acid solution, Electrochim Acta, 70 (2012) 42-49.
[44] S.H. Cadle, Ring-Disk Electrode Study of Palladium Dissolution, J Electrochem Soc, 121 (1974) 645-648.
[45] J.A. Harrison, T.A. Whitfield, The Dissolution of Palladium in Various Electrolytes, Electrochim Acta, 28 (1983) 1229-1236.
[46] J.F. Llopis, L. Victori, J.M. Gamboa, Radiochemical Study of Anodic Behavior of Palladium, Electrochim Acta, 17 (1972) 2225-&.

[47] N. Ibl, G. Gut, M. Weber, Electrodeposition and Catalytic Activity of Palladium Powders, Electrochim Acta, 18 (1973) 307-314.
[48] L.D. Burke, M.B.C. Roche, An Electrochemical Investigation of Monolayer and Multilayer Oxide-Films on Palladium in Aqueous-Media, J Electroanal Chem, 186 (1985) 139-154.
[49] C. Wagner, Kinetik Und Mechanismus Von Umsetzungen Zwischen Flussigen Legierungen Und Schlacken, Z Elektrochem, 62 (1958) 386-389.
[50] R. Schumacher, W. Helbig, I. Haß, M. Wünsche, H. Meyer, The application of fast potential steps to noble metal electrodes: a correlation of electrodissolution with changes in the surface morphology and composition, J Electroanal Chem, 354 (1993) 59-70.
[51] M. Grdeń, J. Kotowski, A. Czerwiński, Study of electrochemical palladium behavior by the quartz crystal microbalance. I. Acidic Solutions, J Solid State Electr, 3 (1999) 348-351.
[52] M. Łukaszewski, A. Czerwiński, Dissolution of noble metals and their alloys studied by electrochemical quartz crystal microbalance, J Electroanal Chem, 589 (2006) 38-45.
[53] Y.M. Kolotyrkin, V.V. Losev, A.N. Chemodanov, Relationship between Corrosion Processes and Oxygen Evolution on Anodes Made from Noble-Metals and Related Metal-Oxide Anodes, Mater Chem Phys, 19 (1988) 1-95.
[54] Y.M. Maksimov, A.V. Smolin, B.I. Podlovchenko, On the ratio of processes of adsorbed oxygen layer formation and palladium surface layer dissolution at linear anodic potential sweep, Russ J Electrochem+, 43 (2007) 1412-1417.
[55] A. Kumar, D.A. Buttry, Size-Dependent Anodic Dissolution of Water-Soluble Palladium Nanoparticles, J Phys Chem C, 117 (2013) 26783-26789.
[56] S. Cherevko, G.P. Keeley, S. Geiger, A.R. Zeradjanin, N. Hodnik, N. Kulyk, K.J.J. Mayrhofer, Dissolution of Platinum in the Operational Range of Fuel Cells, Chemelectrochem, 2 (2015) 1471-1478.
[57] A.A. Topalov, I. Katsounaros, M. Auinger, S. Cherevko, J.C. Meier, S.O. Klemm, K.J.J. Mayrhofer, Dissolution of Platinum: Limits for the Deployment of Electrochemical Energy Conversion?, Angew Chem Int Edit, 51 (2012) 12613-12615.
[58] S. Cherevko, A.A. Topalov, I. Katsounaros, K.J.J. Mayrhofer, Electrochemical dissolution of gold in acidic medium, Electrochem Commun, 28 (2013) 44-46.
[59] S. Cherevko, A.A. Topalov, A.R. Zeradjanin, I. Katsounaros, K.J.J. Mayrhofer, Gold dissolution: towards understanding of noble metal corrosion, Rsc Adv, 3 (2013) 16516-16527.
[60] J. Pritchard, L. Kesavan, M. Piccinini, Q. He, R. Tiruvalam, N. Dimitratos, J.A. Lopez-Sanchez, A.F. Carley, J.K. Edwards, C.J. Kiely, G.J. Hutchings, Direct Synthesis of Hydrogen Peroxide and Benzyl Alcohol Oxidation Using Au-Pd Catalysts Prepared by Sol Immobilization, Langmuir, 26 (2010) 16568-16577.
[61] K.J.J. Mayrhofer, S.J. Ashton, J. Kreuzer, M. Arenz, An Electrochemical Cell Configuration Incorporating an Ion Conducting Membrane Separator between Reference and Working Electrode, Int J Electrochem Sc, 4 (2009) 1-8.
[62] V.I. Birss, M. Chan, T. Phan, P. Vanysek, A. Zhang, An electrochemical study of the composition of thin, compact Pd oxide films, J Chem Soc Faraday T, 92 (1996) 4041-4047.
[63] A.J. Zhang, V.I. Birss, P. Vanysek, Impedance Characterization of Thin Electrochemically Formed Palladium Oxide-Films, J Electroanal Chem, 378 (1994) 63-76.
[64] F.A. Lewis, The Palladium Hydrogen System, Academic Press, (1967).
[65] A.J. Zhang, M. Gaur, V.I. Birss, Growth of Thin, Hydrous Oxide-Films at Pd Electrodes, J Electroanal Chem, 389 (1995) 149-159.
[66] S. Cherevko, N. Kulyk, K.J.J. Mayrhofer, Durability of Platinum-Based Fuel Cell Electrocatalysts: Dissolution of Bulk and Nanoscale Platinum, Nano Energy.

[67] M. Łukaszewski, M. Soszko, A. Czerwiński, Electrochemical Methods of Real Surface Area Determination of Noble Metal Electrodes - an Overview, Int J Electrochem Sc, 11 (2016) 4442-4469.
[68] A. Zalineeva, S. Baranton, C. Coutanceau, G. Jerkiewicz, Electrochemical Behavior of Unsupported Shaped Palladium Nanoparticles, Langmuir, 31 (2015) 1605-1609.
[69] S. Cherevko, N. Kulyk, C.H. Chung, Nanoporous palladium with sub-10 nm dendrites by electrodeposition for ethanol and ethylene glycol oxidation, Nanoscale, 4 (2012) 103-105.
[70] M. Seo, M. Aomi, Piezoelectric Response to Surface Stress Change of a Palladium Electrode in Sulfate Aqueous-Solutions, J Electrochem Soc, 139 (1992) 1087-1090.
[71] M. Tian, B.E. Conway, Phenomenology of oscillatory electro-oxidation of formic acid at Pd: role of surface oxide films studied by voltammetry, impedance spectroscopy and nanogravimetry, J Electroanal Chem, 581 (2005) 176-189.
[72] K. Gossner, E. Mizera, The Anodic Behavior of Pd Electrodes in 1-M H2so4, J Electroanal Chem, 125 (1981) 347-358.
[73] V. Chausse, P. Regull, L. Victori, Formation of a Higher Palladium Oxide in the Oxygen Evolution Potential Range, J Electroanal Chem, 238 (1987) 115-128.
[74] V.I. Birss, V.H. Beck, A.J. Zhang, P. Vanysek, Properties of thin, hydrous Pd oxide films, J Electroanal Chem, 429 (1997) 175-184.
[75] S. Cherevko, A.R. Zeradjanin, G.P. Keeley, K.J.J. Mayrhofer, A Comparative Study on Gold and Platinum Dissolution in Acidic and Alkaline Media, J Electrochem Soc, 161 (2014) H822-H830.
[76] S. Cherevko, A.R. Zeradjanin, A.A. Topalov, N. Kulyk, I. Katsounaros, K.J.J. Mayrhofer, Dissolution of Noble Metals during Oxygen Evolution in Acidic Media, Chemcatchem, 6 (2014) 2219-2223.

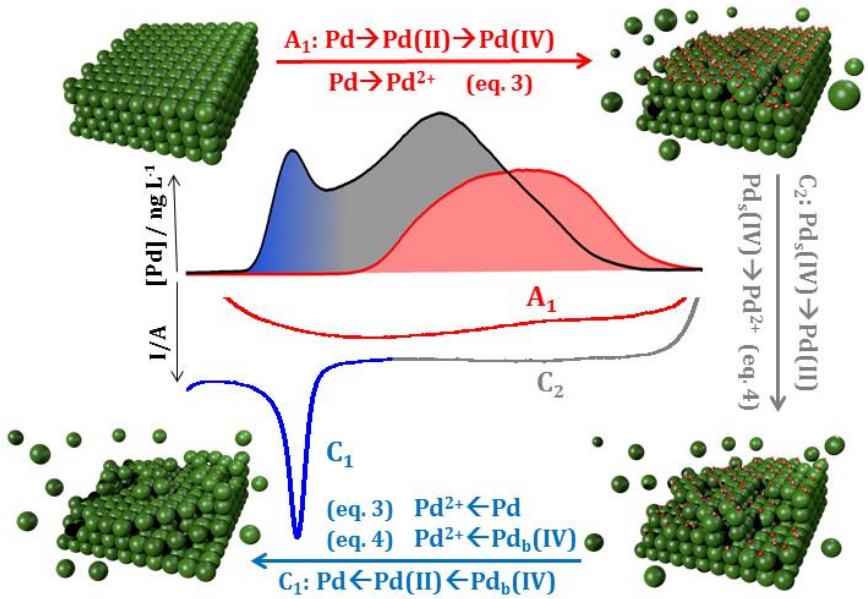


870

871 **Graphical abstract**

872

873

874

875

876

877

878

879

880

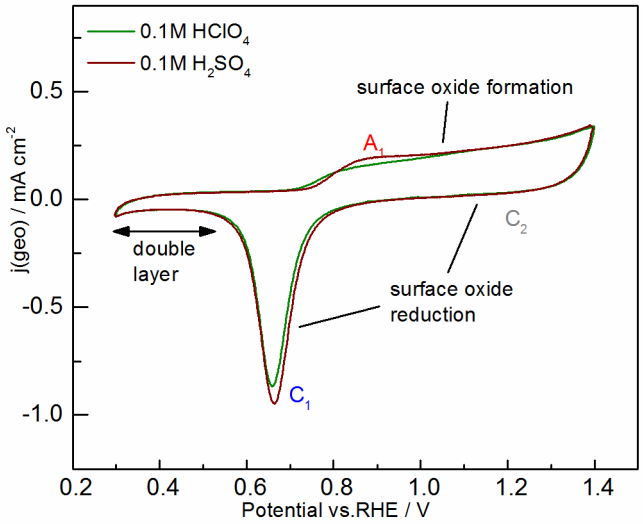


**Figure 1 CVs recorded for a poly-Pd electrode in the SFC setup in 0.1M $HClO_4$ and in 0.1M $H_2SO_4$. Scan rate: 200 mV $s^{-1}$. The position of the anodic oxidation peak and two cathodic reduction peaks are indicated with $A_1$, $C_2$ and $C_1$ respectively. The complete cycle voltammogram (including hydrogen adsorption/absorption and desorption) and the comparison with RDE are reported in the SI.**

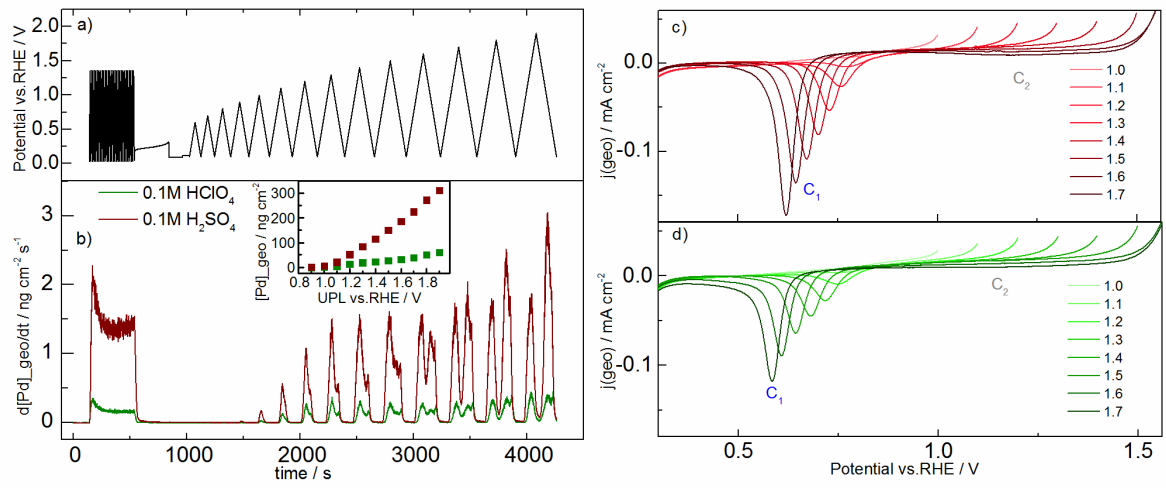


**Figure 2 (a) The potential program applied to the poly-Pd electrode consisted of 30 scans (200 mV $s^{-1}$) for cleaning, an open circuit potential (OCP) phase and several scans (10 mV $s^{-1}$) with increasing UPL. The measured poly-Pd dissolution profiles are shown in (b). The inset in (b) corresponds to the integrated dissolved mass of Pd per cycle at different UPL. The corresponding cathodic sweeps for different UPL in 0.1M $H_2SO_4$ and $HClO_4$ are shown in (c) and (d) respectively. The charge densities associated to the reduction peaks $C_1$ and $C_2$ are shown in the SI.**

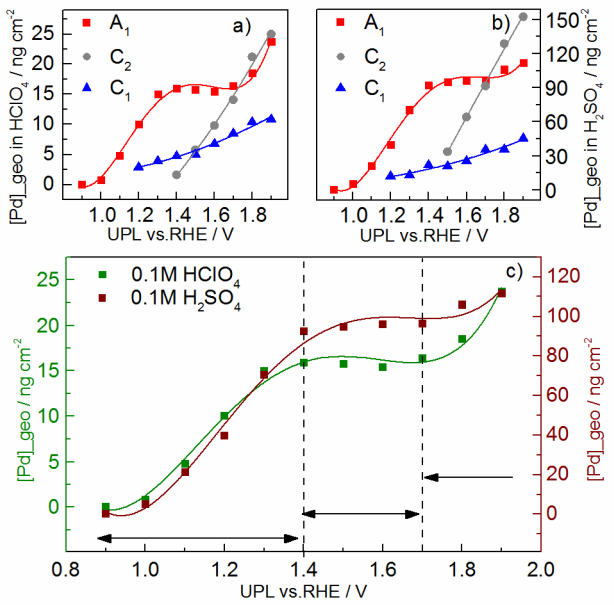


**Figure 3 Integrated mass of dissolved Pd corresponding to the anodic dissolution peak ($A_1$) and the two cathodic peaks ($C_2$ and $C_1$) are reported in $HClO_4$ (a) and $H_2SO_4$ (b) at different UPL during the protocol shown in Figure 2. (c) Comparison of the anodic ($A_1$) dissolution peak in the two acids.**

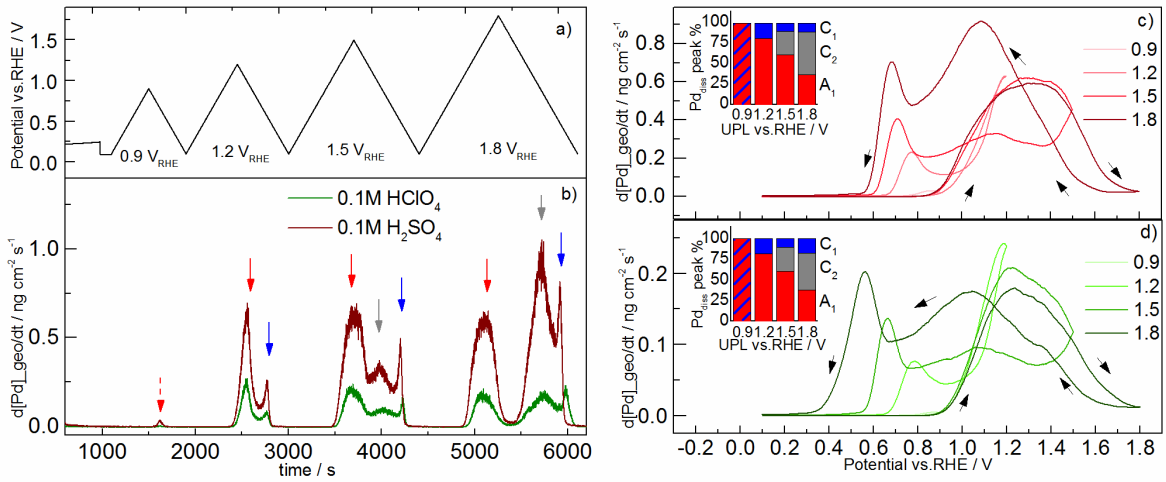


**Figure 4 (a) 4 slow scans (2 mV $s^{-1}$) with increasing UPL (0.9, 1.2, 1.5, 1.8 $V_{RHE}$) and the corresponding measured poly-Pd dissolution profiles in 0.1M $HClO_4$ and $H_2SO_4$ (b). The position of the first (anodic: $A_1$) dissolution peak and the two cathodic ($C_2$ and $C_1$) are marked by red, grey and blue arrows respectively. The corresponding mass cyclic voltammograms in (c) sulphuric and (d) perchloric acid. The percentage of anodic ($A_1$) and cathodic dissolution ($C_2$ and $C_1$) are shown for the respective acid in the inlet of (c) and (d).**

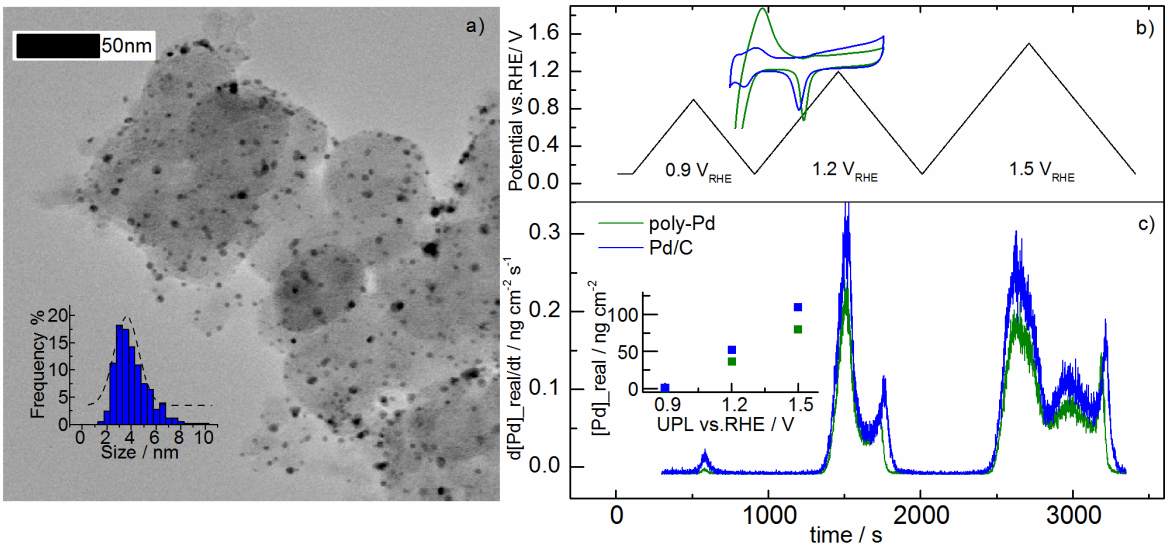


**Figure 5 (a) Bright field TEM micrographs showing Pd/C nanocatalyst deposited on a lacey carbon TEM grid, and their particle size distribution (inset). (b) slow scans (2 mV $s^{-1}$) with increasing UPL and the corresponding measured poly-Pd and Pd/C dissolution profiles normalized by the real surface are (for Pd/C estimated after the activation) (c). Normalized CVs (b-inset) and the normalized mass dissolved per cycle (c-inset) are also shown. Electrolyte: 0.1M $HClO_4$.**

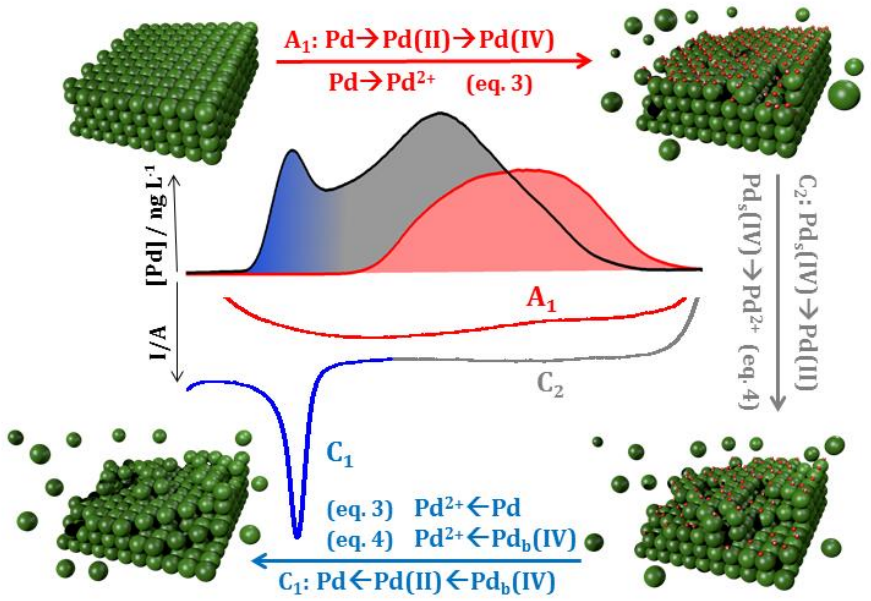


983

984 **Scheme 1 Proposed model of the transient dissolution of Pd. $A_1$: from double**
985 **layer region to Pd-oxide (both Pd(II) and Pd(IV) oxidation states depending on**
986 **the UPL). $C_2$: reduction of Pd(IV)-oxide to Pd(II)-oxide and Pd metal (with**
987 **dissolution). $C_1$: reduction of Pd(II)-oxide to Pd metal.**

988